# Cr-doped TiSe$_2$ – a layered dichalcogenide spin glass

Huixia Luo[1][*], Jason W. Krizan[1], Elizabeth M. Seibel[1], Weiwei Xie[1], Brendan F. Phelan[1], Jing Tao[2], Zhen Wang[3], Jiandi Zhang[3], and R. J. Cava[1][*]

[1]*Department of Chemistry, Princeton University, Princeton, New Jersey 08544, USA.*

[2]*Department of Condensed Matter Physics and Materials Science, Brookhaven*

*National Laboratory, Upton, New York 11973, USA.*

[3]*Department of Physics and Astronomy, Louisiana State University*

*Baton Rouge, La 70803*

**ABSTRACT**

We report the magnetic characterization of the Cr-doped layered dichalcogenide TiSe$_2$. The temperature dependent magnetic susceptibilities are typical of those seen in geometrically frustrated insulating antiferromagnets. The Cr moment is close to the spin-only value, and the Curie Weiss thetas ($\theta_{CW}$) are between -90 and -230 K. Freezing of the spin system, which is glassy, characterized by peaks in the ac and dc susceptibility and specific heat, does not occur until below $T/\theta_{CW} = 0.05$. The CDW transition seen in the resistivity for pure TiSe$_2$ is still present for 3% Cr substitution but is absent by 10 % substitution, above which the materials are metallic and *p*-type. Structural refinements, magnetic characterization and chemical considerations indicate that the materials are of the type Ti$_{1-x}$Cr$_x$Se$_{2-x/2}$ for $0 \leq x \leq 0.6$.

* Corresponding author: R. J. Cava or H.X Luo. E-mail address: rcava@princeton.edu or huixial@princeton.edu

## 1. Introduction

Frustration of magnetic ordering arises in both atomically disordered systems and systems where the magnetic interactions are not compatible with the underlying structural symmetry.[1-5] Classical spin glasses, and systems with magnetic ions on triangular or tetrahedral lattices display such frustration. Materials with strong geometric magnetic frustration are generally electrically insulating or at best strongly semiconducting[5-16] and classical spin glasses can be either metallic or semiconducting. Typically, frustrated magnetic materials are characterized by a Curie-Weiss theta $\theta_{cw}$ that is significantly greater than the spin freezing temperature $T_f$. The frustration index $f = \theta_{cw}/T_f$ is often taken as a general characterization of the degree of frustration.

The $MX_2$ layered transition-metal dichalcogenides (TMDCs, M = Mo, W, V, Nb, Ta, Ti, Zr, Hf, and Re, and X = Se, S or Te) are a large family of solids with layered triangular metal lattices, and have long been of interest due to the rich electronic properties that arise from their low dimensionality. (see, e.g. refs. 17-21) Within the TMDCs, 1T-TiSe$_2$ has attracted special attention due to the presence of a Charge Density Wave (CDW) that onsets at 200 K.[21,22] The material has trigonal symmetry,[23] with TiSe$_6$ octahedra sharing edges in triangular geometry TiSe$_2$ layers that are bonded to each other by Se-Se van der Waals forces (Figure 1a). Here we study the effect of Cr substitution for Ti in 1T-TiSe$_2$.

We find that as Cr atoms are substituted for Ti, they induce metal occupancy in the van der Waals gap between the TiSe$_2$ layers (Figure 1a). We interpret our data to indicate that at concentrations less than about 20 %, the Cr ions primarily occupy the interstitial octahedral sites in the van der Waals layers, but at higher concentrations they occupy both the octahedral interstitial sites and sites in the Ti layers; when they do that they then displace some Ti into the interstitial positions and the system becomes quite disordered. (The materials system is complex: a previous study[24] of Cr-intercalated TiSe$_2$ yielded magnetic properties that are significantly different from those that are observed here, implying that the magnetic behavior of the system may be dependent on synthetic conditions.) Cr ions most frequently are ionic and have the oxidation state Cr$^{3+}$ in solids due to their very strong Hunds-rule coupling.[25] In a material like TiSe$_2$, which is a small band gap semiconductor with a conduction band made from empty Ti $d$ states and a valence band made from filled Se $p$ states (i.e. consisting of Ti$^{4+}$ and Se$^{2-}$), the presence of Cr$^{3+}$ along with Ti$^{4+}$ and Se$^{2-}$ requires a decrease in the Se to metal ratio to below 2:1 and a formula Ti$_{1-x}$Cr$_x$Se$_{2-x/2}$ to

maintain charge neutrality. This picture for Cr-doped $TiSe_2$ is supported by the materials synthesis, the diffraction data, the magnetic data, and the presence of two types of magnetic spins clearly seen in the ac susceptibility for higher $x$ materials.

The DC Magnetic susceptibilities confirm that the Cr moments in $Ti_{1-x}Cr_xSe_{2-x/2}$ are within experimental error of the expected $Cr^{3+}$ spin-only value.[26] The antiferromagnetic Curie-Weiss thetas are large, between -90 and -230 K. The freezing of the spin system, characterized by peaks in the ac and dc susceptibility, occurs between about 2 and 12 K. Resistivity and hall effect measurements on polycrystalline pellets show the suppression of the CDW state in $TiSe_2$ for low values of Cr substitution and metallic, $p$-type conductivity at higher levels of substitution. The complexity of the material system precludes the determination of a detailed model for the magnetism at this stage, but the general feathures are well described by a picture of magnetic disorder on a triangular lattice.

## 2.1 Experimental

Polycrystalline samples of target composition $Ti_{1-x}Cr_xSe_2$ were synthesized by solid state reaction. Mixtures of high-purity fine powders of Ti (99.9 %), Cr (99.95 %), and Se (99.999%) in the appropriate stoichiometric ratios were thoroughly ground, pelletized and heated in sealed evacuated quartz glass tubes at 700 $^o$C for 72 h. Subsequently, the as-prepared powders were reground, re-pelletized and sintered again at 700 $^o$C for 48 h. Powder X-ray diffraction (PXRD, Bruker D8 Advance ECO, Cu Kα radiation) was initially used to structurally characterize the samples. Excess elemental selenium was present in all the synthesis tubes, and easily separated from the sample pellets by sublimation. The presence of the excess Se in the system indicated that the Se:M ratio of the obtained products was less than 2:1, as described further below. Single phase powder samples (after the excess Se was distilled away) were studied by synchrotron X-ray diffraction at the Advanced Photon Source at Argonne National Laboratory on beamline 11-BM. All diffraction patterns were refined using the Rietveld method in the Fullprof software suite.[27]

The DC magnetization (M) as a function of applied magnetic field (H) was linear for all samples up to applied fields of $\mu_0H = 1$ Tesla above the spin glass ordering temperature, and thus the magnetic susceptibility χ was defined as χ = $M/\mu_0H$ at 1 Tesla. Zero-field cooled (ZFC) dc magnetization measurements to obtain χ were performed on heating from 1.8 K to 300 K in a magnetic field of 1 T in a Quantum

Design superconducting quantum interference device (SQUID) equipped Magnetometer (MPMS-XL-5). Temperature dependent magnetizations for selected high Cr content samples were also measured in the MPMS with an applied field of 200 Oe to allow the observation of the bifurcation of the zero field cooled and field cooled magnetizations at the spin freezing transition. Measurements of the temperature dependence of the electrical resistivity, ac magnetic susceptibility, and heat capacity were performed in a Quantum Design Physical Property Measurement System (PPMS). Resistivities and heat capacities below 2 K for selected compositions were measured in the PPMS equipped with a $^3$He cryostat. The nonmagnetic analogue $TiSe_2$ was synthesized and used for the subtraction of the phonon contribution to estimate the magnetic contribution to specific to the specific heat for the Cr-doped $TiSe_2$ materials.

Specimens for transmission electron microscopy (TEM) were obtained from synthesized samples crushed in a dry box and transported to the microscope in ultra-high vacuum. Scanning TEM (STEM) in high-angle annular dark-field (HAADF) mode, energy-dispersive X-ray spectroscopy (EDXS), electron energy-loss spectroscopy (EELS), selected area electron diffraction (SAED), and high-resolution TEM (HRTEM) were conducted in a JEOL 2100F microscope equipped with a liquid-helium cooled sample holder at Brookhaven National Laboratory.

### 3. Results and Discussion

Figure 1b shows the composition dependence of the room temperature lattice parameters for $Ti_{1-x}Cr_xSe_{2-x/2}$ ($0 \leq x \leq 0.6$). $x = 0.6$ is the high Cr composition limit of the intercalated $TiSe_2$-like solid solution. Surprisingly, for $0 \leq x \leq 0.2$, $a$ decreases slightly and $c$ decreases slightly. For $x \geq 0.2$, in contrast, the unit cell parameter $a$ increases with Cr content, and $c$ decreases more quickly. Thus for Cr-doped $TiSe_2$, the composition-dependent unit cell parameters do not follow Vegard's law. This is the fundamental characteristic showing that there is a change in the structure of the system near $x = 0.2$. The complexity is due to the way that the Cr atoms are accommodated in the structure – on Cr substitution, extra metal atoms are found in the Van der Waals gap between in the layers, as described below.

At low Cr doping levels, the powder diffraction data were not very sensitive to the presence of intercalated metals.[28] but for the higher Cr doping levels, quantitative tests of different structural models were possible. In these tests we observed clearly

that the Se sites are fully occupied. This is consistent with what has been found for all layered dichalcogenides of the type $M_xMX_2$ where the X:M ratio is less than 2:1; on doping, metal interstitials are found in the van der Waals gap rather than vacancies in the close packed chalcogen planes.[29] Further, free refinement of the occupancy of the interstitial metal sites led to occupancies that were within the standard error of expectations for the nominal compositions. Thus we conclude that Se sites are fully occupied and that the level of metal intercalation corresponds to the value appropriate to the material composition. The superiority of this model for describing the stucutures of the $Ti_{1-x}Cr_xSe_{2-x/2}$ materials is clearly seen by comparison of Figures 1c and 1d. The fits to the synchrotron X-ray pattern for $Ti_{0.6}Cr_{0.4}Se_{1.8}$ for the interstitial occupancy model (full metal site occupancy in the Ti layer by both Ti and Cr, interstitial ions, and no selenium vacancies) and the alternative Se vacancy model model (full metal site occupancy in the Ti layer by both Ti and Cr, no interstitial ions, and selenium vacancies) are compared. At higher Cr contents than those studied here, the related compound $Cr_4TiSe_8$ has been reported to have two magnetic transitions, at $T_f$ = 50 K and $T_N$ = 120 K.[30] In our magnetic measurements, we did not see those transitions in any samples (See Figure 3) indicating that this compound is not present as an impurity in our materials. The diffraction data analysis, the requirements of charge neutrality, and the presence of excess Se in the synthetic system indicates that the best way to represent the composition of the fabricated compounds is $Ti_{1-x}Cr_xSe_{2-x/2}$, which we use here. (An equivalent, though more complex formula reflecting the observed crystal structure, which shows the presence of both interstitial metal atoms and full Se site occupancy, would be $Cr_{y/3}(Ti_{1-y}Cr_y)Se_2$, where the leading Cr is intercalated and the metal atoms in parentheses are those in the normal dichalcogenide layers; the relation between this and the simpler formula employed here is $[y+y/3]/[1+y/3] = x$.)

For more detailed structural characteriozation, in order to check for possible Cr clustering or nanoscale precipitates in Cr doped $TiSe_2$, which would impact the magnetism of the system, high-resolution transmission electron microscopy (HRTEM) was used to examine one of the high Cr content materials, $Ti_{0.6}Cr_{0.4}Se_{1.8}$. Figure 2a shows the crystal structure model for the [100] zone for this material, where the Ti/Cr atoms (grey balls) are in octahedral coordination with Se (yellow balls). Figures 2b and 2c show the HAADF-STEM image for the [100] zone at different magnifications and the inset of Figure 2b, top, is the selected area electron diffraction (SEAD) pattern

along a [100] zone axis. Figure 2d shows the HAADF-STEM image for the [001] zone and the inset of Figure 2d on top is the SAED pattern in the [001] zone. The STEM-HAADF micrographs in Figure 2b-d as well as the SAED patterns reveal a homogenous Cr distribution in $Ti_{0.6}Cr_{0.4}Se_{1.8}$; no clusters or nano-scale Cr-precipitates were observed. Figures 2d-i show the EELS spectra obtained at each pixel during scanning in the boxed area. Intensities of the core-loss edge of each element were integrated and mapped in the scanning area to show the Ti, Cr and Se elemental distribution at the atomic level. The element maps images further confirm that there is no segregation or clustering of Cr in $Ti_{0.6}Cr_{0.4}Se_{1.8}$, even at the atomic level. Therefore there is a homogenous distribution of Cr within the structure.

Figure 3a shows the zero-field cooled temperature (T) dependence, from 1.8 to 300 K, of the dc magnetic susceptibility ($\chi$) for the $Ti_{1-x}Cr_xSe_{2-x/2}$ polycrystalline samples. The plot of $\chi$ versus T in Figure 3a shows increasing $\chi$ with decreasing T for all samples and the inset shows that the magnetic susceptibility increases linearly with Cr concentration at a fixed temperature; this is a qualitative indication of the fact that the Cr has a constant magnetic moment across the series. Figure 3b shows the character of the AFM transition under the relatively low applied field of 200 Oe. The antiferromagnetic (AFM) transition temperature increases with increasing Cr content for $x \leq 0.4$. for higher Cr doping, however, the AFM transition, while still seen, becomes broad and poorly defined.

Figure 4a shows the temperature dependent inverse susceptibilities, $1/(\chi - \chi_0)$ vs. T, constructed from the data shown in Figure 3a. In the high temperature region, above 200 K, all magnetic susceptibilities ($\chi$) can be fit to $\chi - \chi_0 = C / (T - \theta_{CW})$, where C is the Curie constant, $\theta_{CW}$ is the Curie-Weiss temperature, and $\chi_0$ is the temperature independent contribution to the susceptibility. The fits were performed in the temperature range between 200 and 300 K; linear relationships (shown as solid lines in Figure 4a) were found for all $Ti_{1-x}Cr_xSe_{2-x/2}$ compounds above 200 K. $\chi_0$ is negligible and set to 0 for all but the lowest Cr content studied, $x = 0.03$. The effective magnetic moment ($P_{eff}$) per Cr ion can be obtained by using $P_{eff} = (8C)^{1/2}$. The Curie-Weiss temperature is an estimate of the net magnetic interaction strength; the $\theta_{cw}$s are larger in magnitude than -90 K for all materials. In $Ti_{0.75}Cr_{0.25}Se_{1.875}$, for example, $\theta_{cw}$ is -174 K and no magnetic transition is apparent until approximately 2.5 K, giving this material a frustration index $f$ of ~70, indicating that $Ti_{0.75}Cr_{0.25}Se_{1.875}$ is strongly

frustrated. The effective moment per Cr, $P_{eff}$, is ~ 4 $\mu_B$ and is observed to be only weakly dependent on Cr concentration. The $\theta_{CW}$ values, however, increase in magnitude with increasing Cr content (see the inset of Figure 4a, top).

To better compare the magnetic characteristics of all members of the $Ti_{1-x}Cr_xSe_{2-x/2}$ ($0.03 \leq x \leq 0.6$) family, we rearrange the Curie-Weiss Law to the normalized form $C/(\chi|\theta_{cw}|)=T/|\theta_{cw}|-1$. Plots of the magnetic data in this form are especially useful in comparing the general behavior of geometrically frustrated magnets.[1,2,31] The result is a dimensionless plot of the normalized inverse susceptibility against normalized temperature for all samples - the susceptibility is scaled by the magnitude of the moments (C) and the Temperature is normalized by the strengths of the magnetic interactions ($|\theta_{cw}|$).[31] Ideal antiferromagnets would have a slope of 1 and intercept of the y axis at 1 in this representation (shown as a solid green line y = x + 1 in Figure 4b), with indications of magnetic ordering on the order of $T/\theta_{cw}$ ~ 0.5 - 1. Antiferromagnetic or ferromagnetic correlations at lower temperatures in excess of those expected for simple Curie-Weiss behavior are manifested as positive or negative deviations respectively from the green solid line y = x + 1, respectively. This allows differences in the nature of correlations above $T_N$ to be identified and easily compared among different materials. It can be seen in the figure that the $Ti_{1-x}Cr_xSe_{2-x/2}$ system maintains nearly ideal Curie-Weiss behavior to normalized temperatures near 1.2 $T/\theta_{cw}$ before exhibiting increased ferromagnetic fluctuations just before its spin freezing transition, which occurs well below a $T/\theta_{cw}$ of 0.05. The plot shows that the higher Cr doping compositions show larger relative ferromagnetic deviations from the green line. The ferromagnetic deviations from the antiferromagnetic Curie-Weiss law in the frustrated regime, at $T/\theta_{cw} = 0.1$, are illustrated in the inset of Figure 4b.

The low temperature dc and ac susceptibilities of $Ti_{0.5}Cr_{0.5}Se_{1.75}$ near the magnetic freezing transition are presented in Figure 5. Figure 5a shows the dc susceptibility under an applied 200 Oe field, which indicates that the transition temperature is 8-9 K. Figure 5b presents the ac susceptibility under an applied field of 20 Oe at different frequencies. On this plot, we can see that the transition temperature $T_f$ shifts to higher temperature as the frequency of the ac field increases (10 Hz data omitted for clarity), which is a characteristic trait of spin glasses.

No hysteresis is observed in the M(H) data at 2 K recorded during increasing and decreasing cycles of magnetic field. In addition, it can be seen that the data shows

slight curvature, but is nowhere near saturation within the accessible field range. A broad peak is seen in the ac susceptibility data in the 7 - 12 K temperature range, characteristic of spin freezing. Figure 5c shows the field-dependent magnetization, (as M vs. $\mu_0$H) at 2 K. The ratio of the shift in transition temperature ($\Delta T_f$) to the transition temperature ($T_f$) times the log of the change in frequency ($\Delta \log f$) used in the expression of $\Delta T_f/(T_f \Delta \log f)$, which parameterizes the dependence $T_f$ on $f$, can be used to characterize spin glasses, and spin glass like materials.[32] Based on the ac susceptibilities, taking the transition temperature as the maximum of $\chi'$ in Figure 5b, we obtain $p = \Delta T_f/(T_f \Delta \log f) = 0.004$, which is much smaller, for example, than that of insulting pyrochlore $NaCaCo_2F_7$ (where $p = 0.029$), however it is very similar to what is seen for metallic alloy spin glasses such as MMn (M = Cu, Au, Ag, around 0.005).[33,34] To further parameterize the spin glass behavior, the frequency ($f$) dependence of $T_f$ can be fitted by the empirical Volger-Fulcher law with the equation:

$\tau = \frac{1}{f} = \tau_0 exp \frac{Ea}{k_b(T_f-T_0)}$, where $T_f$ is the freezing temperature, $f$ is the frequency, $\tau_0$ is the intrinsic relaxation time, $E_a$ is the activation energy of the process, and $T_0$ is "the ideal glass temperature".[35,36] After rearranging the Volger-Fulcher law, a simple relation between $T_f$ and $f$ with the presentation of $T_f = T_0 - \frac{E_a}{k_b}\frac{1}{\ln(\tau_0 f)}$ can be used. Figure 5d shows the resulting fits. The intrinsic relaxation time ($\tau_0$) cannot be fitted for the current data, and thus selected values were used varying from 1 x $10^{-7}$ s (super-paramagnets, cluster glasses) [37] to 1 x $10^{-13}$ s (conventional spin glasses).[38] When $\tau_0$ was set to a value of 1 x $10^{-7}$ s, we obtain $E_a = 7.17$ x $10^{-4}$ eV and $T_0 = 8.48$ K, yielding $E_a/k_B = 2.14$. Setting the intrinsic relaxation time $\tau_0$ to be the smallest value, 1 x $10^{-13}$ s, we obtain $E_a = 4.57$ x $10^{-3}$ eV, $T_0 = 7.10$ K and the value of $E_a/k_B = 53$. Finally, if $\tau_0 = 1$ x $10^{-12}$ s, a mid-range value, is assumed, we obtain $E_a = 3.70$ x $10^{-3}$ eV, $T_0 = 7.33$ K and the ratio $E_a/k_B = 43$.

Further characterization of the freezing of the spins was perfrmed via heat capacity measurements. Figure 6 shows in the main panel the raw heat capacity data for $Ti_{1-x}Cr_xSe_{2-x/2}$ (x = 0, 0.25, 0.5), presented as Cp/T vs. T for T between 2 and 120 K. Estimates of the magnetic specific heat can be obtained by performing a subtraction of the $TiSe_2$ data from that of the Cr doped materials after normalization by 2% such that the Cp/T values match at temperatues of 100 K and higher. This subtravted dta is shown in the inest to Figure 6. A sharp ordering feature is not seen in the heat capacity, consistent with a picture where the spins freeze in a random

configuration.[36] Rough integration of the magnetic heat capacities indicates that the the total integrated entropy values are low compared to those expected for two-state or S = 3/2 Heisenberg systems, (Rln(2) or Rln(2S+1)) and thus that the spin freezing observed in the magnetic susceptibility does involve all of the spins; there may be considerable residual magnetic entropy in the $Ti_{1-x}Cr_xSe_{2-x/2}$ system below 2 K.

Finally, the temperature dependence of the electrical resistivities, plotted as the $\rho/\rho_{300K}$ ratios for polycrystalline $Ti_{1-x}Cr_xSe_{2-x/2}$ ($0.03 \leq x \leq 0.6$) are shown in Figure 7. All the Cr-doped samples have resistivities below 6 mohm cm at 300 K. The ratios ($\rho/\rho_{300K}$) for $Ti_{1-x}Cr_xSe_{2-x/2}$ ($0.03 \leq x \leq 0.6$) were less than 1 (Figure 7a), excepting for the lowest doping ($x = 0.03$) in this case. For $x = 0.03$, the signature of CDW transition ($T_{CDW}$) was obvious in around 125 K, which is lower that found in undoped 1T-$TiSe_2$ (where $T_{CDW} \approx 200$ K). Meanwhile, we can see that the CDW was suppressed with higher Cr doping; the $Ti_{1-x}Cr_xSe_{2-x/2}$ compounds become more metallic. The samples found to be $p$-type by Hall coefficient measurements (not shown) with carrier concentrations in the range of 2-7 x $10^{20}$ $cm^{-3}$, typical of those found for heavily doped small band gap semiconductors, as expected.

## 4. Conclusion

Cr-substituted $TiSe_2$ materials of the form $Ti_{1-x}Cr_xSe_{2-x/2}$ ($0.03 \leq x \leq 0.6$) have been synthesized successfully via a solid state reaction method. TEM studies confirm that there are no Cr clusters or Cr-rich particles in this system. The X-ray diffraction refinements indicate that Cr goes into the Van der Waals gap position. Based on the partial substitution of Cr for Ti in $Ti_{1-x}Cr_xSe_{2-x/2}$, $Cr^{3+}$ on the triangular-planar geometry lattice leads to the frustration of the magnetic ordering: we have observed no long-range magnetic ordering at low temperatures. The Curie-Weiss thetas $\theta_{cw}$ were much greater than the freezing temperatures $T_f$s, confirming that the system is highly frustrated. The system appears to be similar to systems such as $Sr_{1-x}Eu_xS$[37], where both disorder-induced and geometry-induced frustration of the magnetic ordering are present, with the exception that the present system is metallic with low carrier concentration. More detailed studies of the charge transport and magnetism in this complex system would be of further interest.

**References**

1. John E. Greedan, Geometrically frustrated magnetic materials, *J. Mater. Chem.*, **2001**, 11, 37±53.

2. R. Moessner and A. R. Ramirez, Geometrical frustration, *Physics Today* **2006**, 59, 24-29.

3. S. T. Bramwell and M. J. P. Gingras, Spin Ice State in Frustrated Magnetic Pyrochlore Materials, *Science* **2001**, 294, 1495-1501.

4. Gardner, J. S.; Gingras, M. J. P.; Greedan, J. E. Magnetic pyrochlore oxides, *Reviews of Modern Physics* 2010, 82, 53-107.

5. A.P. Ramirez, Strongly Geometrically Frustrated Magnets, *Annu. Rev. Mater. Sci.* **24** 453 (1994).

6. Bramwell, S. T.; Gingras, M. J. P. Spin Ice State in Frustrated Magnetic Pyrochlore Materials, *Science* 2001, 294, 1495-1501.

7. Fennell, T.; Deen, P. P.; Wildes, A. R.; Schmalzl, K.; Prabhakaran, D.; Boothroyd, A. T.; Aldus, R. J.; McMorrow, D. F.; Bramwell, S. T. Magnetic Coulomb Phase in the Spin Ice $Ho_2Ti_2O_7$ , *Science*, 2009, 326, 415- 417.

8. Morris, D. J. P.; Tennant, D. A.; Grigera, S. A.; Klemke, B.; Castelnovo, C.; Moessner, R.; Czternasty, C.; Meissner, M.; Rule, K. C.; Hoffmann, J.-U.; Kiefer, K.; Gerischer, S.; Slobinsky, D.; Perry, R. S. Dirac Strings and Magnetic Monopoles in the Spin Ice $Dy_2Ti_2O_7$, *Science*, 2009, 326, 411-414.

9. J. W. Krizan and R. J. Cava, $NaCaCo_2F_7$: A single-crystal high-temperature pyrochlore antiferromagnet, *Phys. Rev.B,* 2014, **89,** 214401-214405.

10. Kemei, M. C.; Moffitt, S. L.; Darago, L. E.; Seshadri, R.; Suchomel, M. R.; Shoemaker, D. P.; Page, K.; Siewenie, J. Structural ground states of $(A,A')Cr_2O_4$ (A = Mg, Zn; A′ = Co, Cu) spinel solid solutions: Spin-Jahn-Teller and Jahn-Teller effects, *Phys. Rev. B,* 2014, 89, 174410-174424.

11. Aeppli, G.; Broholm, C.; Ramirez, A.; Espinosa, G. P.; Cooper, A. S. Broken spin rotation symmetry without magnetic Bragg peaks in Kagome antiferromagnets*, Journal of Magnetism and Magnetic Materials*,1990, 90–91, 255.

12. Ramirez, A. P.; Espinosa, G. P.; Cooper, A. S. Strong frustration and dilution-enhanced order in a quasi-2D spin glass**,** *Physical Review Letters* **1990**, *64*, 2070-2073.

13. Obradors, X.; Labarta, A.; Isalgué, A.; Tejada, J.; Rodriguez, J.; Pernet, M. Magnetic frustration and lattice dimensionality in $SrCr_8Ga_4O_{19}$, *Solid State Communications*, 1988, 65, 189.

14. Rigol, M.; Singh, R. R. P. Magnetic Susceptibility of the Kagome Antiferromagnet $ZnCu_3(OH)_6Cl_2$, *Physical Review Letters* 2007, 98, 207204.

15. Helton, J. S.; Matan, K.; Shores, M. P.; Nytko, E. A.; Bartlett, B. M.; Yoshida, Y.; Takano, Y.; Suslov, A.; Qiu, Y.; Chung, J. H.; Nocera, D. G.; Lee, Y. S. Spin Dynamics of the Spin-1/2 Kagome´ Lattice Antiferromagnet $ZnCu_3(OH)_6C_{l2}$, *Physical Review Letters* 2007, 98, 107204.

16. Shores, M. P.; Nytko, E. A.; Bartlett, B. M.; Nocera, D. G. A Structurally Perfect S=1/2 Kagome´ Antiferromagnet, *J Am Chem Soc*, 2005, 127, 13462-13463.

17. Wilson J. A, Yoffe A.D. The transition metal dichalcogenides discussion and interpretation of the observed optical, electrical and structural properties. *Adv Phys* 18:193 (1969).

18. M. M. Ugeda; A. J Bradley; S.-F. Shi; F. H. da Jornada; Y. Zhang; D. Y. Qiu; W. Ruan; S.-K. Mo; Z. Hussain; Z.-X. Shen; F. Wang; S. G. Louie; M. F Crommie, Giant bandgap renormalization and excitonic effects in a monolayer transition metal dichalcogenide semiconductor, *Nat Mater*, 2014, 13, 1091

19. Soumyanarayanana A., Yee Michael M., He Y., van Wezel J., Rahne Dirk J., Rossnagel K., Hudson E. W., Norman Michael R., and Hoffman J. E, Quantum phase transition from triangular to stripe charge order in $NbSe_2$, *PNAS* 110:1623 (2013).

20. Luo H. X., Xie W. W. , Tao J., Inoue H., Gyenis A., Krizan J. W. , Yazdani A., Zhu Y. M., and Cava R. J., Polytypism, polymorphism, and superconductivity in $TaSe_{2-x}Te_x$, *Proc Natl Acad Sci* USA, 2015, 112(11), E1174-E1180.

21. Di Salvo, F. J.; Moncton, D. E.; Waszczak, J. V. Electronic properties and superlattice formation in the semimetal $TiSe_2$, *Phys. Rev. B,* 1976, 14, 4321-4328.

22. Stoffel, N. G.; Kevan, S. D.; Smith, N. V. Experimental band structure of 1T-$TiSe_2$ in the normal and charge-density-wave phases, *Phys. Rev. B,* 1985, 31, 8049-8055.

23. Oftedal, I. Roentgenographische Untersuchungen von $SnS_2$ , $TiS_2$ , $TiSe_2$ , $TiTe_2$. *Z. Phys. Chem.* 1928, 134, 301-310.

24. Pleschov, V.G., Baranov, N.V., Titov, A.N., Inoue, K., Bartashevich, M.I., and Goto, T., Magnetic Properties of Cr-intercalated $TiSe_2$, J. Alloys and Cmpds. 320 13 (2001).

25. Georges, A.; Medici, L. d.; Mravlje, J., Strong Correlations from Hund's Coupling, Annual Review of Condensed Matter Physics 2013, 4, 137.

26. Myers, H.P., Introductory Solid State Physics, Taylor and Francis, London 1997, p. 336

27. Gaulin, B. D. Magnetic materials: The texture of frustrated magnets, *Nat Mater,* **2005**, *4*, 269-270.

28. A powder X-ray refinement cannot differentiate unambiguously between Cr and Ti as their scattering factors are very similar. Although the structure is well determined, the ratio of Ti to Cr in the two metal sites (i.e. in the van der Waals gap and in the Ti-plane) could not be specified from the structural refinement of the the diffraction data.

29. J. L. Beeby, P. K. Bhattacharya, P. Ch. Gravelle, F. Koch, D. J. Lockwood, Condensed Systems of Low Dimensionality, springer, Volume 253,1991, p677-678.

30. Rodríguez-Carvajal J., Recent developments of the program FULLPROF, *Comm. Powder Diffr.* **2001**, 26, 12-19.

31. Bensch, W.; Sander, B.; Näther, C.; Kremer, R. K.; Ritter, C. Synthesis, crystal structure, magnetic properties and spin glass behaviour of the new ternary compound $Cr_4TiSe_8$, *Solid State Sciences* **2001**, *3*, 559.

32. S.E. Dutton, E.D. Hanson, C.L. Broholm, J.S. Slusky, and R.J. Cava, Magnetic properties of hole-doped SCGO, $SrCr_8Ga_{4-x}M_xO_{19}$ (M = Zn, Mg, Cu), *J. Phys. Condens. Matter* 2011, **23**, 386001.

33. J.A. Mydosh and I. Ebrary, Spin Glasses: An Experimental Introduction (Taylor & Francis London, 1993).

34. Shtrikman, S.; Wohlfarth, E. P. The theory of the Vogel-Fulcher law of spin glasses, *Phys. Lett. A* **1981**, 85, 467-470.

35. Aharoni, A. The Vogel-Fulcher law of spin glasses, *Phys. Lett. A* **1983**, *99*, 458-460.

36. Bhowmik, R. N.; Ranganathan, R. Anomaly in cluster glass behaviour of $Co_{0.2}Zn_{0.8}Fe_2O_4$ spinel oxide, *Journal of Magnetism and Magnetic Materials* **2002**, *248*, 101-111.

37. Tholence, J. L. On the frequency dependence of the transition temperature in spin glasses, Solid State Communications, **1980**, 35, 113-117.

38. Ramirez, A. P.; Hayashi, A.; Cava, R. J.; Siddharthan, R.; Shastry, B. S. Zero-point entropy in 'spin ice', *Nature* **1999**, 399, 333-339.

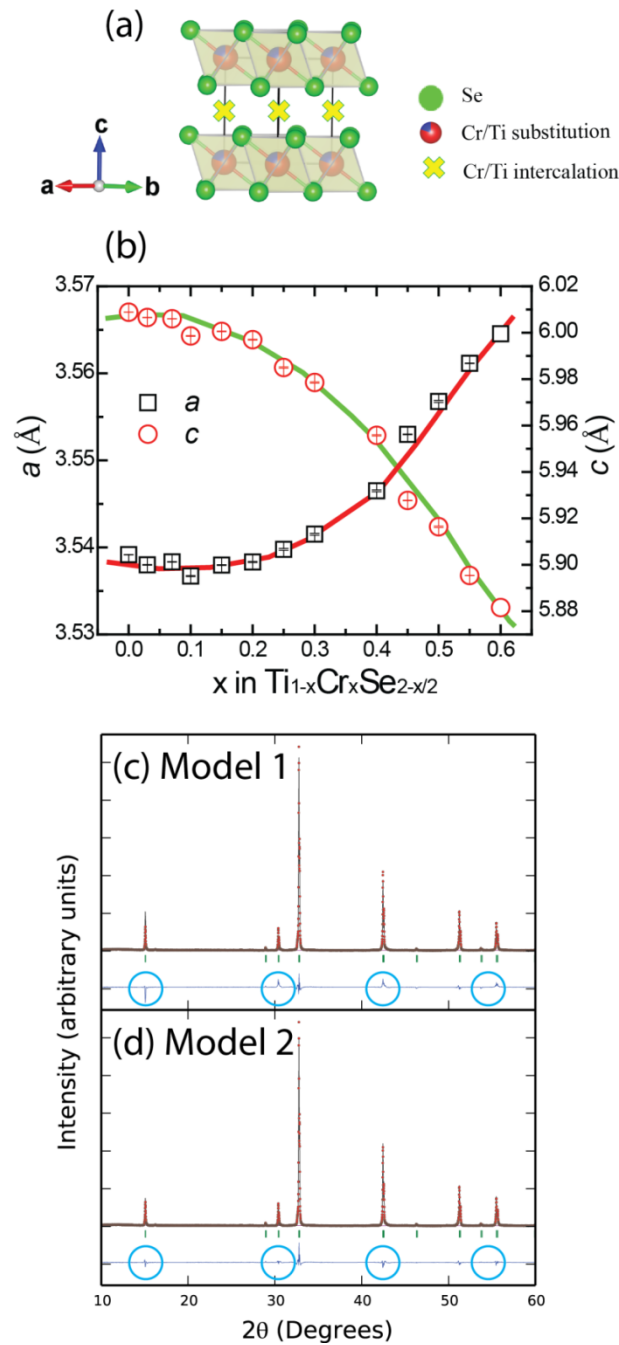39. H. Maletta, spin glass properties of (Eu,Sr)S, *J. de. Physique colloques* **41 (C5)** 115 (1980).

**Figure 1. Structural characterization of 1T-Ti$_{1-x}$Cr$_x$Se$_{2-x/2}$.** (a and b) The overall crystal structure of 1T-TiSe$_2$ (a), (b) Composition dependence of the room temperature lattice parameters $a$ and $c$ for Ti$_{1-x}$Cr$_x$Se$_{2-x/2}$ ($0 \leq x \leq 0.6$), (c) and (d) refined powder Xray diffraction data for the two structural models for Ti$_{0.4}$Cr$_{0.6}$Se$_{1.7}$. The superioriy of the model for metal interstitials (Model 2) over selenium vacancies (Model 1) is seen through comparison of the difference plots. Regions of interest are marked by circles.
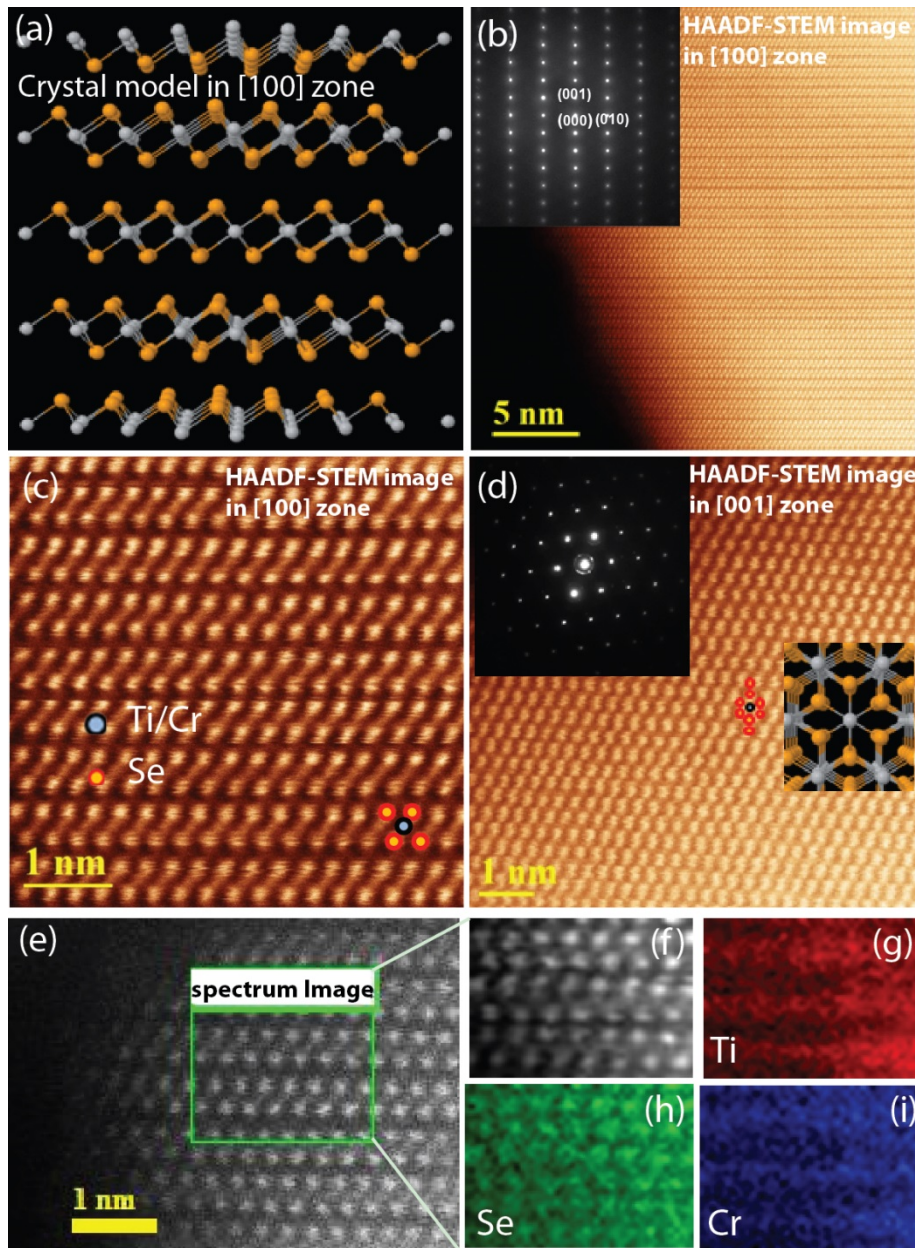
**Figure 2**. **High-resolution transmission electron microscopy (HETEM) characterization of 1T-Ti$_{0.6}$Cr$_{0.4}$Se$_{1.8}$** (a) crystal model in the [100] zone; (b) and (c) HAADF-STEM image in the [100] zone at different magnifications; (d) HAADF-STEM image in the [001] zone; (e)-(i) Electron energy loss spectroscopy (EELS) spectra (g-i) obtained at each pixel during scanning in the boxed area (e,f). Intensities of the core-loss edge of each element were integrated and mapped in the scanning area to show the elemental distribution at the atomic level. No segregation of Cr was found.
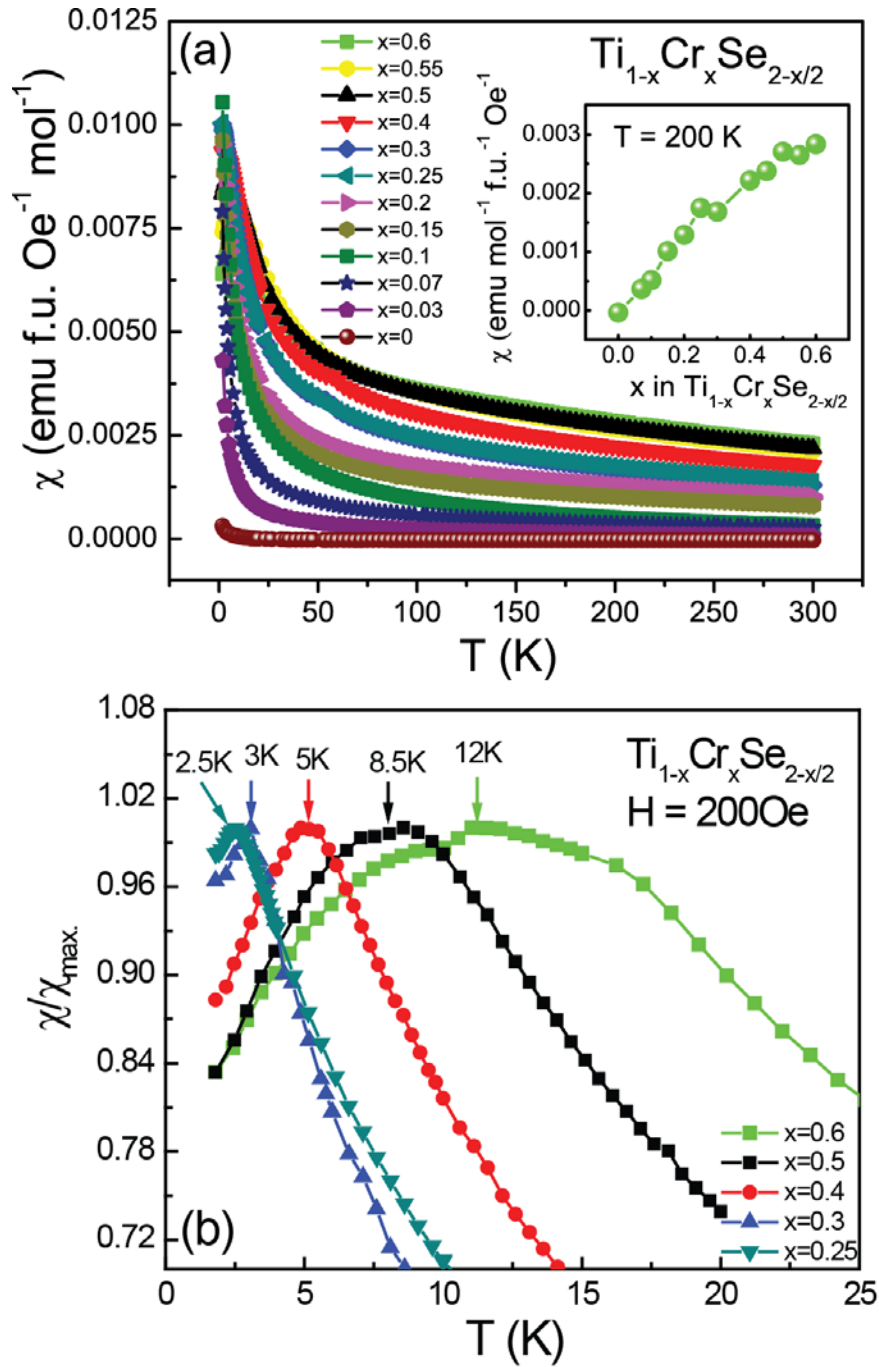
**Figure 3**. **General Magnetic characterization of $Ti_{1-x}Cr_xSe_{2-x/2}$** (a) Magnetic susceptibility ($\chi$) versus temperature for $Ti_{1-x}Cr_xSe_{2-x/2}$ ($x = 0$, 0.07, 0.15, 0.2, 0.25, 0.3, 0.4, 0.5, 0.6). Inset $\chi$ at 200 K vs. $x$ for $Ti_{1-x}Cr_xSe_{2-x/2}$. (b) Normalized $\chi/\chi_{max}$ versus temperature in a 200 Oe field for $Ti_{1-x}Cr_xSe_{2-x/2}$ ($x = 0.25$, 0.3, 0.4, 0.5, 0.6).
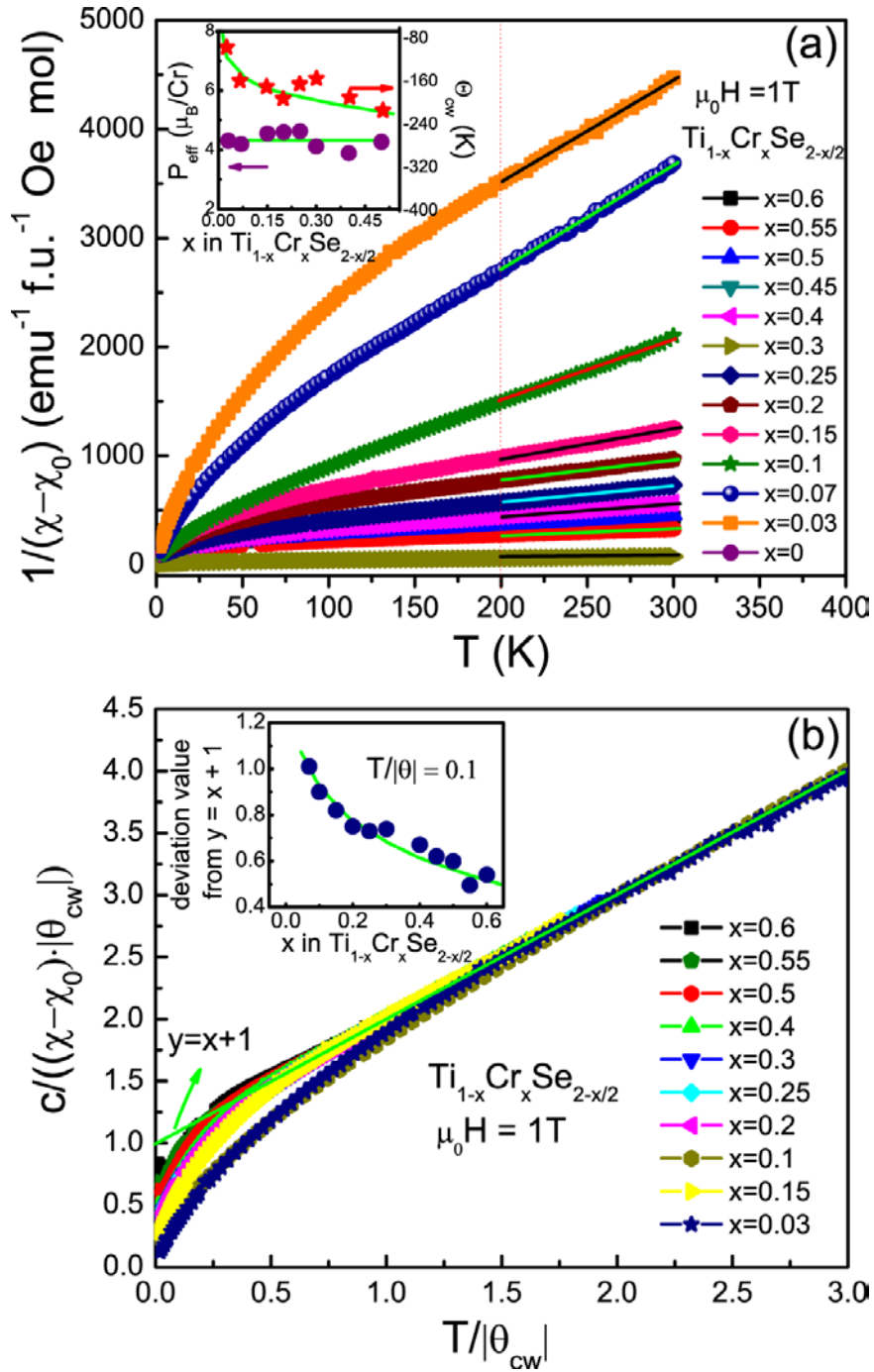
**Figure 4**. **Curie-Weiss plots for Ti$_{1-x}$Cr$_x$Se$_{2-x/2}$.** (a) Inverse susceptibility (1 / $\chi$ - $\chi_0$) versus temperature in a 1 T field for Ti$_{1-x}$Cr$_x$Se$_{2-x/2}$. Inset: effective moment and Curie Weiss temperatures. (b) Plot of C/|$\theta_{cw}$|($\chi$-$\chi_0$) versus T/|$\theta_{cw}$| for Ti$_{1-x}$Cr$_x$Se$_{2-x/2}$ ($x$ = 0.03, 0.07, 0.15, 0.2, 0.25, 0.3, 0.4, 0.5). This plot shows that these compounds exhibit consistent Curie behavior at high temperatures.
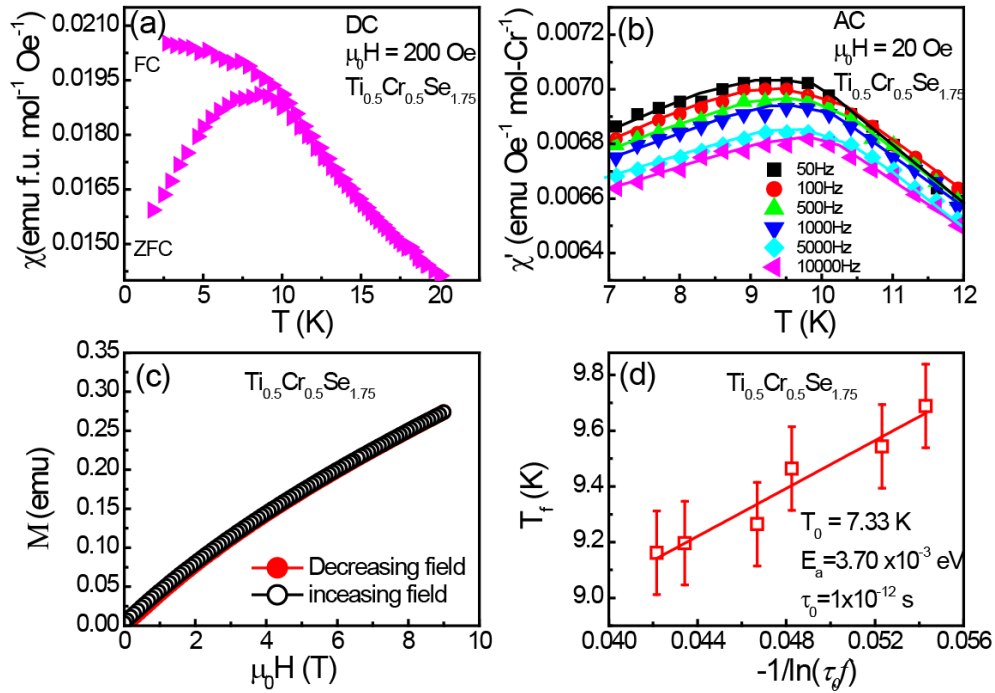
**Figure 5. Spin glass characterization of $Ti_{1-x}Cr_xSe_{2-x/2}$** (a) Temperature dependence of the dc susceptibility in an applied field of 200 Oe for $Ti_{0.5}Cr_{0.5}Se_{1.75}$. (b) Temperature dependence of the ac susceptibility in an applied field of 20 Oe for $Ti_{0.5}Cr_{0.5}Se_{1.75}$ as a function of frequency. (c) M-H curve for $Ti_{0.5}Cr_{0.5}Se_{1.75}$ at 2 K. (d) The behavior parameterized in a fit to the Volger-Fulcher law.

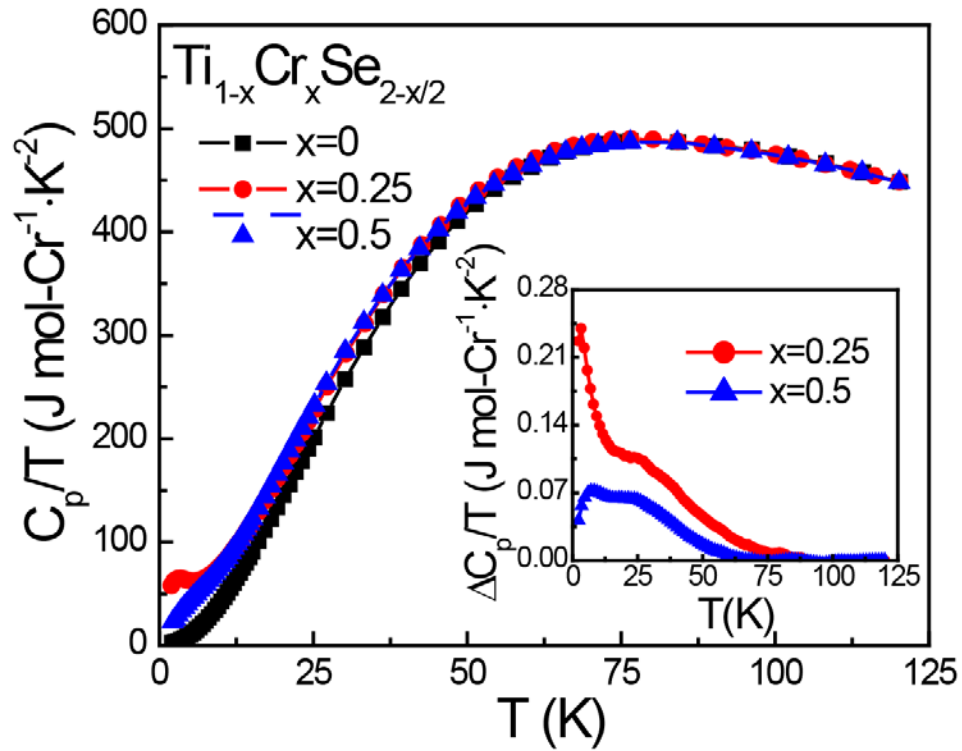**Figure 6**. **Heat capacity characterization of Ti$_{1-x}$Cr$_x$Se$_{2-x/2}$.** Main Panel: heat capacity of Ti$_{1-x}$Cr$_x$Se$_2$ (x = 0, 0.25, 0.5) in the form of Cp/T over a wide temperature range. The prsensence of extra entropy at low temperarture for the Cr-doped materials is clearly seen. Inset: The temperature dependence of the excess heat capacity of Ti$_{1-x}$Cr$_x$Se$_2$ (x = 0.25, 0.5), determined by the subtraction of the heat capacity of TiSe$_2$. This heat capacity must be a reflection of the spin freezing in the system.
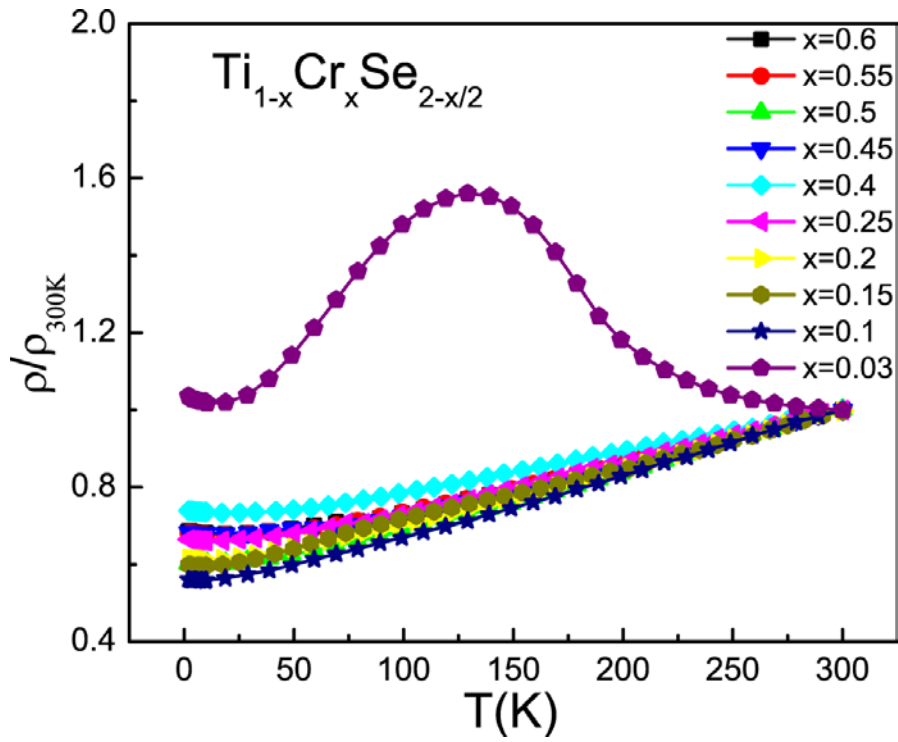
**Figure 7**. **Characterization of the resistivity of $Ti_{1-x}Cr_xSe_{2-x/2}$**. The temperature dependence of the ratios ($\rho/\rho_{300K}$) for polycrystalline pellets of $Ti_{1-x}Cr_xSe_{2-x/2}$ ($0.03 \leq x \leq 0.6$).